Free Energy Reconstruction in Bidirectional Force Spectroscopy Experiments: The Effect of the Device Stiffness

Simone Marsili and Piero Procacci*

Dipartimento di Chimica, Universita di Firenze, Via della Lastruccia 3, I-50019 Sesto Fiorentino, Italy, and Centro Interdipartimentale per lo Studio delle Dinamiche Complesse (CSDC), Via Sansone 1, I-50019 Sesto Fiorentino, Italy

Received: September 8, 2009; Revised Manuscript Received: December 9, 2009

In force spectroscopy single-molecule experiments, an individual molecule, usually a polymer, is mechanically stretched by means of an externally controlled driving potential. Typically, the stiffness of this potential is much smaller than the stiffness of the potential of mean force along the molecular extension coordinate. Here we discuss how such a disparity alters the free energy and the reversibility of the driven system, with respect to the pristine molecular system under examination. In particular, by simulating unfolding/refolding experiments of a small protein, we examine the traits of the potential of mean force that are responsible for the dramatic amount of work dissipated in experiments using a soft device. Finally, we show that in bidirectional experiments the free energy of the free molecular system can be easily recovered by appropriate reweighting methods.

Introduction

Single-molecule mechanical manipulations in atomic force microscopy (AFM) or optical trap (OT) experiments provide a powerful means for investigating the structural and dynamical properties of biological molecules. In these experiments, a single molecular construct, for example, a protein attached on both sides to flexible "molecular handles",[1] is tethered from one end to a fixed support while the other end is subject to the harmonic potential exerted by a cantilever in AFM or by the optical trap produced by a highly focused laser beam. The system device interaction potential is thus of the form

$$V(r-\lambda)=\frac{K}{2}(r-\lambda)^2 \tag{1}$$

where r is the fluctuating molecular extension, and λ is the position of the trap/cantilever center that can be controlled by the experimenter. K, the force constant, is typically of the order of few pN nm^{-1} for an AFM apparatus and even less (0.1−0.5 pN nm^{-1}) for an optical trap. Displacement of the device translates in the motion of the rest position λ of the microscopic spring, the trap pipet distance in OT experiments or the cantilever center support distance in the AFM experiment. The resulting force returned to the instrument is due to the mechanical resistance of the molecular construct to the applied stretching tension. In a single protein, the resistance to an externally imposed mechanical stretching stress is clearly related to its folding free energy.[1−6] Typically, the applied external force is raised until a culminating transition event occurs (i.e., unfolding of a protein subdomain, unzipping of a DNA hairpin). In such cases, rupture-force histograms can be used to fit lifetimes, free energy activation barriers, and distances to transition states.[5] The experiments can often be inverted (i.e., one can refold) by using the same experimental apparatus, strained proteins,[7] or unfolded DNA sequences.[3] The work measured by the device in an unfolding experiment is given by

$$W=\int_{\lambda_F}^{\lambda_U} F(\lambda,r)\mathrm{d}\lambda \tag{2}$$

where $F(\lambda,r)=-K(r-\lambda)$ is the force measured by the instrument, and λ_F and λ_U are two device positions that correspond, respectively, to a folded and an unfolded state of the polymer. This work can be used directly in the work fluctuation theorem (WFT)[3,8,9] expression to recover the free energy difference between the initial and final states characterized by the fixed λ_F and λ_U values of the experimental control parameter λ. The WFT reads

$$\frac{P_U(W)}{P_F(-W)}=\mathrm{e}^{\beta(W-\Delta G)} \tag{3}$$

where $P_U(W)$ is the probability to spend the work W in an unfolding experiment, $P_F(-W)$ is the probability to perform the work $-W$ in the reverse process (refolding) with inverted time protocol; $\beta=1/k_BT$ with T being the bath temperature. $\Delta G=G(\lambda_U)-G(\lambda_F)$ is the free energy difference between the final and initial states of the molecule plus device system in an unfolding process, where $G(\lambda)=-k_BT\ln Z(\lambda)$ and $Z(\lambda)$ is the canonical partition function:

$$Z(\lambda)=\int \mathrm{d}x\mathrm{e}^{-\beta H(x,\lambda)} \tag{4}$$

with x denoting a vector in phase space. $H(x,\lambda)=H_m(x)+(K/2)(r-\lambda)^2$ is the Hamiltonian for the system and comprises the molecular energy $H_m(x)$ and the molecule device interaction $V(r-\lambda)$.

Actually, rather than in $G(\lambda)$ one is interested in the free energy profile $G_m(r)=-k_BT\ln Z_m(r)$ along the molecular extension coordinate r that is directly related to the probability $P_m(r)$ of a given value of r when sampling from the canonical ensemble corresponding to the molecular Hamiltonian H_m (i.e., excluding the contribution from the device):

* To whom correspondence should be addressed. E-mail: procacci@chim.unifi.it.

10.1021/jp908663z
Published on Web 02/01/2010

$$P_m(r) = Z_m^{-1} Z_m(r) = Z_m^{-1} \int dx e^{-\beta H_m(x)} \delta[r - r(x)] \quad (5)$$

The relation between $G_m(r)$ and $G(\lambda)$ can be easily worked out; the canonical probability $P(r|\lambda)$ of a molecular extension r, while the device is held fixed in λ is given by

$$P(r|\lambda) = e^{\beta G(\lambda)} e^{-\beta G_m(r)} e^{-\beta V(r-\lambda)} \quad (6)$$

where we have used the definition $G(\lambda) = -k_B T \ln Z(\lambda)$. Therefore, $G_m(r)$ and $G(\lambda)$ are related by the equation

$$G(\lambda) = G_m(r) + V(r - \lambda) + k_B T \ln P(r|\lambda) \quad (7)$$

The functions $G_m(r)$ and $G(\lambda)$ are practically coincident if the force constant K of the instrument is much stiffer[10] with respect to the stiffness $K_m(r) = (\partial^2 G_m(r)/\partial r^2)$ of the molecular potential of mean force (PMF) $G_m(r)$. This is clearly not so in AFM or OT experiments, where the force constant K is small compared to the stiffness of the potential of mean force $G_m(r)$ in the vicinity of the native state. The latter for α-helix[11] or RNA hairpin can be of the order $K_m = 10^4 - 10^5$ pN nm^{-1}. In such cases, as pointed out in several past studies,[12,13] $G_m(r)$ may differ substantially from $G(\lambda)$.

In this study, we realistically simulate, using classical molecular dynamics (MD) simulations, the steered unfolding and refolding of an α-helical protein in vacuo. By comparing these results to simulations of the same system done with an extremely stiff force constant, we show that the experimentally determined value of the unfolding free energy $G(\lambda)$ differs dramatically from the actual molecular PMF $G_m(r)$, fully confirming the findings of a very recent experimental study.[14] We further rationalize and discuss the phenomenology of single-molecule experiments in the "soft" device case by examining the behavior of the unfolding and refolding work distributions and of the hysteresis as a function of the pulling speed and of the device stiffness, showing how the instrument potential in eq 1 makes the system with Hamiltonian $H(x, \lambda) = H_m(x) + V(r - \lambda)$ much less reversible along the driven r coordinate with respect to the molecular system. Finally, we show that the free energy difference ΔG_m between the extended and the folded state of the molecule can be easily recovered from the free energy difference ΔG of the driven system, without resorting to the recently proposed PMF reconstruction[12,13] procedures involving the weighted histogram analysis method.[12,15]

Simple Mechanical Model of a Single-Molecule Experiment. We begin by considering a simple model of loading a molecule with a harmonic potential. Generally, the native and the fully extended states of a molecular system correspond to convex regions of the PMF, and we will approximate these states as harmonic oscillators. In the scheme of Figure 1, the single molecule is therefore represented by a harmonic spring with force constant K_m and equilibrium distance r_m, corresponding to the native or to the unfolded free energy minimum, attached to a fixed support on its left end and to the device spring with force constant K on the right end. The reduced mass associated with the spring stretching coordinate is concentrated on the right terminal bead. The end-to-end molecular distance r (i.e., the extension of the molecular spring) corresponds to the distance of the bead from the fixed support. The device spring on the right accounts for the harmonic driving potential and can be stretched or compressed moving the device, thus propagating the resulting force to the molecular spring.

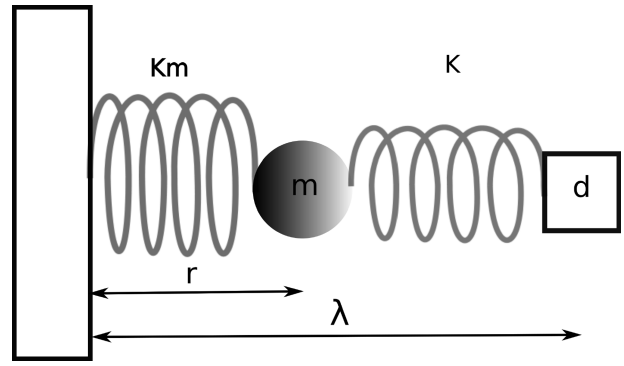

Figure 1. Scheme of an AFM force spectroscopy experiment. The molecule is represented by a harmonic spring with force constant K_m and with the mass concentrated in r on the bead labeled m. The square labeled with the letter d symbolizes the device, which interacts with the molecule with a harmonic potential with force constant K. The unfolding/refolding experiments are performed by driving externally the position λ of the device.

The equation of motion for the molecular extension r during the experiment is given by

$$m\ddot{r} = -K_m r - K(r - \lambda(t)) \quad (8)$$

with $\lambda(t)$ being the rest position of the device spring measured from the fixed support to the cantilever tip. For simplicity, the initial position of the device is considered to be $\lambda(0) = r_m = 0$. Assuming that the cantilever/optical trap is moved at constant pulling speed such that $\lambda(t) = vt$, then the solution of eq 8 is given by

$$r(t) = (\omega/\Omega)^2 vt + A\cos(\Omega t + \phi) \quad (9)$$

where A and ϕ are constants determined by the initial conditions of each trajectory, $\Omega^2 = \omega^2 + \omega_m^2$, and $\omega = (K/m)^{1/2}$ and $\omega_m = (K_m/m)^{1/2}$ are the harmonic frequencies of the device and of the molecular spring, respectively. The time-dependent force measured by the instrument can then be computed using the last relation, and the force/extension relation $F(\lambda)$ is obtained by substituting $t = \lambda/v$:

$$F(\lambda) = K[(\omega_m/\Omega)^2 \lambda - A\cos(\Omega\lambda/v + \phi)] \quad (10)$$

Therefore, if the molecular potential along the end-to-end coordinate can be described by a harmonic spring, the average force $\bar{F}$ registered in a series of experiments starting from equilibrium canonical conditions depends linearly on the device extension coordinate λ

$$\bar{F}(\lambda) = K\left(\frac{\omega_m}{\Omega}\right)^2 \lambda = K_{eff}\lambda \quad (11)$$

where K_{eff} is the effective force constant for the system of two springs in series, $K_{eff}^{-1} = K^{-1} + K_m^{-1}$. In a typical single-molecule experiment, we are in the soft case $K \ll K_m$, and hence $K_{eff} \simeq K$:

$$F(\lambda) \simeq K[\lambda - A\cos(\Omega\lambda/v + \phi)] \quad (12)$$

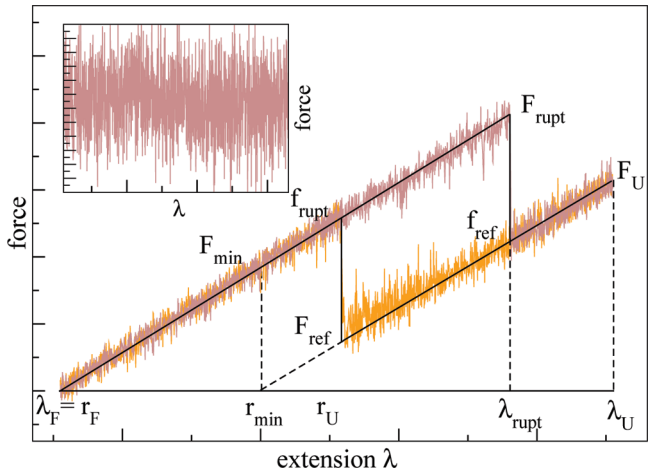

Figure 2. Scheme of typical force/extension plots for a unfolding (brown) and refolding (orange) experiments in the $K_m \gg K$ case. The average force/extension plots in the folded and unfolded PMF branches are shown as black lines with the same slope equal to $K_{eff} \simeq K$. The symbols F_{rupt} and F_{ref} denote, respectively, the rupture force in the unfolding experiment and the refolding force in the folding experiment, and r_F and r_U are the equilibrium average molecular extensions for device positions λ_F and λ_U, respectively. The intercept r_{min} of the force trace on the λ axis corresponds to the position of an eventual minimum in the unfolded branch of the PMF. The rupture force, due to the finite speed of the unfolding experiment, is expected to occur at an extension that is significantly larger than r_U. F_U is the externally applied force that maintains the system at r_U. The frequencies of the work modulations are proportional to the harmonic frequency of the molecular spring. The "stiff" case $K \gg K_m$ is illustrated in the inset. In this case, the frequency of the force modulations is proportional to the harmonic frequency of the device spring, and no sudden rupture of the folded structure is observed. The work spent in an unfolding (W^U) or in a folding (W^F) experiment can be measured as the area under their respective force/extension plots.

such that the slope of a force/extension plot is equal to the *device* force constant K and the molecular force constant K_m can be recovered by evaluating the power spectrum of $F(\lambda)$ that exhibits a single nonzero frequency at $2\pi\nu \simeq \omega_m/v$. This case is presented in the scheme of Figure 2, where typical force/extension plots for unfolding/folding experiments are shown. In the unfolding case (brown line), the applied force grows linearly with the device extension λ until a rupture event happens, with λ well beyond the unfolded molecular extension r_U. When a rupture occurs, the applied force abruptly decreases from F_{rupt} to f_{ref}, the force value corresponding to an extended configuration of the polymer and to the device position at rupture, λ_{rupt}. From thereon, the phenomenology is very similar to that observed before the rupture as the stiffness of the extended polymer is much larger than that of the device. A similar behavior has been observed for the unfolding of Kinesin,[7] the leucine zipper,[7] the m-RNA hairpin.[3]

In computer experiments, one rather works in the opposite regime, that is, under the so-called stiff spring approximation[10] ($K \gg K_m$), such that $K_{eff} \simeq K_m$. In this case one obtains

$$F(\lambda) \simeq K_m[\lambda - A\cos(\Omega\lambda/v + \phi)] \tag{13}$$

and the slope of the force/extension plot corresponds to the molecular force constant K_m while the nonzero frequency of the force power spectrum is $2\pi\nu \simeq \omega/v$. This behavior is illustrated in the inset of Figure 2. More generally, during an unfolding experiment with $K \gg K_m$, the mean applied tension simply reflects the derivative of the molecular PMF $G_m(r)$. Some common traits of force/extension curves as measured in single-molecule experiments can therefore be rationalized in terms of a simple mechanical model based on the coupling of a soft and a hard spring. In the following, we show that the dependence of the free energy ΔG and of the hysteresis of the experiment on the device stiffness K can be made explicit.

In bidirectional experiments, the available measurements are partitioned between both directions (e.g., folding and unfolding). We denote with $r_F = \int dr\, rP(r|\lambda_F)$ the equilibrium average molecular extension in the folded state and with $r_U = \int dr\, rP(r|\lambda_U)$ the average molecular extension obtained with the device maintained in $\lambda = \lambda_U$. Since both folding and unfolding experiments start from equilibrium conditions, the quantities $P(r = r_F|\lambda_F)$ and $P(r = r_U|\lambda_U)$ can be easily evaluated by sampling the initial molecular extension in the unfolding and folding experiments, respectively. Therefore, using eq 7 twice with $\lambda = r_U$ and with $\lambda = r_F$ and subtracting term by term the resulting equations, we find that the free energy difference between the folded and extended state of the polymer, $\Delta G_m = G_m(r_U) - G_m(r_F)$, can be related to the reversible work $\Delta G = G(\lambda_U) - G(\lambda_F)$ spent in driving the device from λ_F to λ_U as

$$\Delta G - \Delta G_m = \Delta V + k_B T \ln \frac{P(r_U|\lambda_U)}{P(r_F|\lambda_F)} \tag{14}$$

where $\Delta V = V(r_U - \lambda_U) - V(r_F - \lambda_F)$ is known a priori. If the distributions $P(r|\lambda_F)$ and $P(r|\lambda_U)$ can be regarded as Gaussian distributions with variances σ_F^2 and σ_U^2, then $P(r_U|\lambda_U)/P(r_F|\lambda_F) = \sigma_F/\sigma_U$, and eq 14 can be rewritten as

$$\Delta G - \Delta G_m = \Delta V - k_B T \ln \frac{\sigma_U}{\sigma_F} \tag{15}$$

The above equation provides a clear physical interpretation of the difference between ΔG and ΔG_m. The term ΔV corresponds to the difference of the device system interaction energy between the initial native and the final extended states, while the second term measures the difference in the spatial spread of the final and initial equilibrium states of the transformation and can be recognized as the entropy change $\Delta S = k_B \ln(\omega_F/\omega_U)$ between two harmonic oscillators with natural frequencies $\omega_F = (k_B T/m)^{1/2}\sigma_F^{-1}$ and $\omega_U = (k_B T/m)^{1/2}\sigma_U^{-1}$.

Generally, λ_F is chosen such that it corresponds to the folded minimum in the molecular PMF along r and therefore $\lambda_F = r_F$. Moreover, for realistic molecular free energy profiles, the second term on the right-hand side of eq 15 can usually be neglected with respect to ΔG_m. In these conditions, eq 15 predicts that the apparent free energy difference of the system plus device with force constant K is given by

$$\Delta G = \Delta G_m + \frac{F_U^2}{2K} \tag{16}$$

where $F_U = K(\lambda_U - r_U)$ is the mean applied force necessary to maintain the system in the unfolded configuration with an average molecular extension r_U, that is

$$F_U = K(\lambda_U - r_U) = K_U(r_U - r_{min}) \tag{17}$$

where K_U is the molecular stiffness of the PMF of the molecular system in the extended configuration and r_{min} is the intercept

of the applied force on the λ axis, corresponding to a hypothetical free energy minimum in the unfolded branch of the molecular PMF $G_m(r)$ (see Figure 2).

On the basis of eq 16, one can derive an expression for the unfolding/folding mean dissipation as a function of K valid in the soft regime. For the sake of simplicity, in the following, we will assume the curvature of the molecular free energy profile $G_m(r)$ to be the same in the folded and unfolded branches and equal to their average, $K_m = (K_F + K_U)/2$. The work spent in an unfolding experiment can be measured as the area under the force/extension curve, see Figure 2:

$$W^U = \frac{F_{min}F_{rupt}}{K_{eff}} + \frac{F_U^2}{2K_{eff}} - \frac{F_{min}^2}{2K_{eff}} \tag{18}$$

where F_{rupt} is the fluctuating rupture force in the unfolding experiment and $F_{min} = K_{eff}r_{min}$. Averaging eq 18 over all unfolding trajectories and subtracting from the result the expression for the free energy difference ΔG in eq 16, one recovers an expression for the mean dissipated work in an unfolding experiment as a function of the mean rupture force $\bar{F}_{rupt}$:

$$W_D^U = \frac{F_{min}\bar{F}_{rupt}}{K_{eff}} - \frac{F_{min}^2}{2K_{eff}} - \Delta G_m \tag{19}$$

We can straightforwardly derive an analogous equation for the dissipated work in a folding experiment as a function of the mean refolding force $\bar{F}_{ref}$, simply inverting the sign of eq 19 and substituting $\bar{F}_{rupt}$ with $\bar{f}_{rupt} = \bar{F}_{ref} + F_{min}$ (see Figure 2):

$$W_D^F = -\frac{F_{min}\bar{F}_{ref}}{K_{eff}} - \frac{F_{min}^2}{2K_{eff}} + \Delta G_m \tag{20}$$

Finally, the mean hysteresis of an unfolding-refolding cycle of measurements, $h = W^U + W^F$, can be recovered by summing eq 19 and eq 20 obtaining

$$h = \frac{F_{min}}{K_{eff}}(\bar{F}_{rupt} - \bar{F}_{ref} - F_{min}) = r_{min}(\Delta F - K_{eff}r_{min}) \tag{21}$$

For this simple model, in which recrossing events are neglected, this equation correctly predicts that $\Delta F = \bar{F}_{rupt}^U - \bar{F}_{ref}^F = F_{min}$ for $h = 0$; that is, the difference between the mean rupture force in the unfolding experiment and the mean refolding force in the folding experiment is equal to F_{min} in the limit of a reversible transformation (see Figure 2). In eq 21, the force difference $\Delta F(K,v)$ is, in general, a function of the force loading rate $\dot{F} = Kv$,[2,4] and $K_{eff} = KK_m/(K + K_m)$.

Computational Details

The "molecular spring" in this study is the typical guinea pig of recent steered molecular dynamics simulation for testing the Jarzynski equality and WFT,[10,11,16] the alanine decapeptide (A_{10}) in vacuo. As we shall see in the forthcoming discussion, in spite of its simplicity, this system exhibits force spectroscopy patterns that are commonly observed in real experiments. The A_{10} molecule is described with the all-atom force field CHARMM, whose parameters are given in ref 17. Previous steered molecular dynamics studies,[8,9] done with this potential function on A_{10} in vacuo, have shown that, at ordinary temperatures, the Helmholtz free energy $G_m(r)$ as a function of the N−N end-to-end distance r exhibits, in the range $15.0 < r < 33.0$ Å, a single minimum at $r = 15.5$ Å corresponding to a three-turn α-helical structure. The second derivative of the free energy with respect to r at the minimum has been found to be[10,11] $K_m \simeq 10^3$ pN nm^{-1} and can be identified with the molecular force constant of the α-helix stretching.

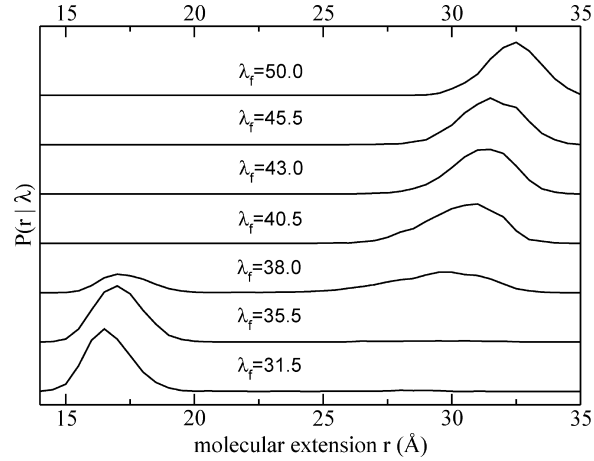

Figure 3. Equilibrium probability densities $P(r|\lambda)$ of the molecular extension r in A_{10} in vacuo at $T = 300$ K for different positions λ of the device: 31.5, 35.5, 38.0, 40.5, 43.0, 45.5, 50.0 Å.

The nonequilibrium simulations of a single A_{10} were conducted at constant temperature using a Nosé-Hoover thermostat.[18] We point out that, in such conditions, application of the Crooks theorem[3] yields the Helmholtz free energy. All of the calculations are performed using an in-house parallel version of the program ORAC.[19,20] The nonequilibrium simulation of a single-molecule stretching experiment from the folded (α-helical) to an extended (*all-trans*) structure and vice versa have been conducted according to the following well-established protocol:[10,11] the N atom of the N-terminus residue has been constrained to a fixed position, while the N atom of the C-terminus residue has been constrained to move along a given fixed direction. The reaction coordinate is hence taken to be the distance between the N atoms of the two terminal amide groups. The C-terminus atom has been subjected to a harmonic potential of adjustable equilibrium position λ of the form of eq 1, mimicking the action of a soft harmonic spring connecting the molecular system with the experimental device. Therefore, λ corresponds to the position of the cantilever in an AFM experiment or the center of the optical trap in an OT experiment.

Results and Discussion

We performed three different series of 512 unfolding and 512 folding driven molecular dynamics, using three different pulling/pushing velocities, $v = 2.67,\ 0.67,\ 0.33$ nm ns^{-1}. The device force constant K in these series of simulations is set to 56 pN nm^{-1}, a value that is typical for an AFM experiment, and much smaller than the underlying molecular spring constant K_m.[11] The unfolding simulations of A_{10} have been performed by moving the device from $\lambda_F = 15.5$ Å, corresponding to the mean value of the r coordinate in the unperturbed helical state, to a distance λ_U that ensures that A_{10} is in the all-trans configuration (corresponding to a r value near 31−32 Å). In Figure 3, we show the equilibrium distribution $P(r|\lambda)$ of the

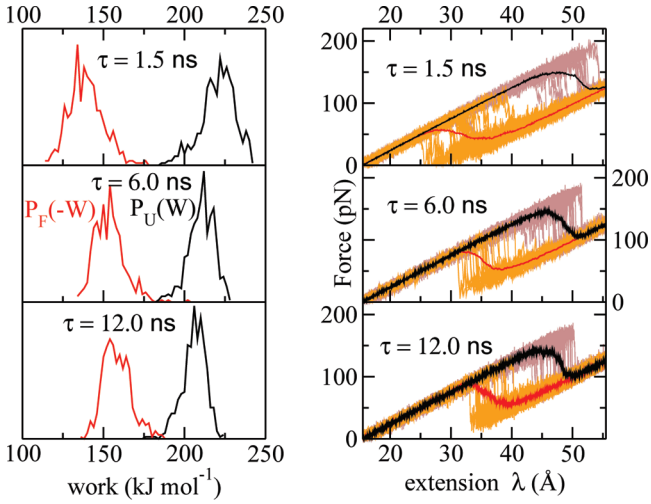

Figure 4. Results of a simulated force spectroscopy experiment on A_{10} at constant device force constant of 56 pN nm^{-1} and at various pulling speeds. Left panel: work distributions for unfolding (black curve) and folding (red curve) experiments at various pulling/pushing speed for A_{10} in vacuo at $T = 300$ K, obtained using 512 forward and reverse independent cycles with the control parameter varying between $\lambda_F = 15.5$ Å and $\lambda_U = 55.5$ Å and using a soft device spring constant of 56 pN nm^{-1}. Right panel: corresponding force/extension plot for a sample of unfolding (brown) and refolding (orange) cycles in A_{10}. The black and red curves are the average forward and reverse force traces, respectively.

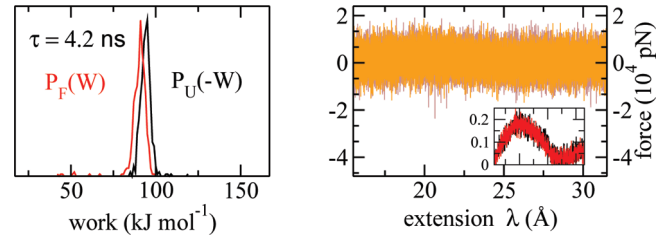

Figure 5. Left panel: Unfolding (black curve) and folding (red curve) work distributions obtained from 512 independent cycles at a constant pulling speed of 0.4 nm ns^{-1} for A_{10} in vacuo at $T = 300$ K. The experiments were performed using a stiff device spring constant of 560 000 pN nm^{-1}.

molecular extension in A_{10} in vacuo at $T = 300$ K obtained from standard molecular dynamics simulation for different positions of the device. For $\lambda \leq 35.5$, the distributions show a single maximum at $r < 20$ Å, corresponding to the α-helix minimum. For $\lambda > 40$ Å, the stable configuration is the extended all-trans configuration, corresponding to the region of the free energy with positive curvature for $r > 27$ Å (see Figure 6). In order to observe a rupture event at each forward realization, we have driven the device position from $\lambda_F = 15.5$ Å to $\lambda_U = 55.5$ Å at constant pulling speed v. The folding experiments were performed using a protocol inverted in time, moving the device at constant speed from $\lambda_U = 55.5$ Å to $\lambda_F = 15.5$ Å. The initial states for these trajectories were sampled at regular time intervals of ∼30 ps during two equilibrium simulations, while fixing the device position at $\lambda_F = 15.5$ Å and $\lambda_U = 55.5$ Å, and using the instrumental force constant $K = 56$ pN nm^{-1}. The results of the nonequilibrium runs are collected and summarized in Figure 4. In the left panel, we plot the work distribution $P_U(W)$ and $P_F(-W)$ for the unfolding and folding sets of experiments, for the three operational pulling−pushing speed. The driven unfolding of the A_{10} peptide yields force/extension plots (right panel of Figure 4) where the force grows linearly as predicted in the soft device case, showing a strong hysteresis (measured as the sum of the average folding and unfolding works) that decreases with decreasing speed. We found for $v = 2.67$, 0.67, and 0.33 nm ns^{-1}, a hysteresis of 39.8, 28.9, and 24.2 kJ mol^{-1}, respectively. The values of the average curvature of the PMF K_m, together with the value of r_{min}, can be measured from the slope and the intercept, respectively, of these force/extension plots, resulting in $K_m = 400$ pN nm^{-1} and $r_{min} = 2.9$ nm.

The nonequilibrium unfolding of the A_{10} system *in vacuo*, for soft control device ($K_m \gg K$), can be thus described fairly accurately by the simple model of two springs in series. This comes actually with no surprise as the end-to-end coordinate r, in the vicinity of the native and extended state and in absence of solvent, is expected to behave like a pure eigenvector with negligible friction effects from the remainder of the degrees of freedom of the polypeptide. In Figure 5, we show the result of a simulation of the same system and in the same conditions with a stiff spring device, using a force constant $K = 560\,000$ pN nm$^{-1} \gg K_m$, for which the control device parameter λ is always close to the driven end-to-end coordinate r. These are the usual computer experiment conditions, based on the so-called stiff spring approximation, whereby G_m may be identified with G.[10]

Comparison of the behavior of A_{10} when the device spring is soft (Figure 4) and stiff (Figure 5) reveals that, while the driven process with stiff force constant basically shows no hysteresis (see Figure 5) at speeds as fast as 0.4 nm ns^{-1}, the process done with a soft force constant shows a very pronounced and persistent hysteresis at comparable or even smaller speeds. In fact, the system driven with the soft spring device shows two wide work distributions with negligible overlap. For example, the area of the hysteresis loop for the series of bidirectional experiments on A_{10} done at the lowest speed of $v = 0.33$ nm ns^{-1} (see Figure 4 right bottom panel) still amounts to about 26% of the mean and reverse forward work, that is, only slightly less than the value found with double speed (central right panel in Figure 4). The origin of such large hysteresis can be understood looking at the equilibrium distributions $P(r|\lambda)$ in Figure 4. When the device is held fixed at $\lambda = 38$ Å, A_{10} toggles between two metastable states, meaning that the potential of mean force $G_m(r) + (K/2)(r - \lambda)^2$ displays a maximum that was not present in the original free energy $G_m(r)$. In Figure 6, this function is shown along with the $G_m(r)$ for three different values of the control parameter. For $\lambda = 38$ Å, the free energy of the system comprising the harmonic driving potential is effectively bistable, and the system is observed to swap between a distorted α-helix and the extended all-trans configuration. The passage from one state to the other requires the surmounting of a wide barrier of several k_BT, an indeed rare event in *a single molecule* at ordinary temperature. In such conditions, statistical equilibrium may take a long time to establish. This in turn implies that, in nonequilibrium experiments, the system becomes more "irreversible"at intermediate values of the r coordinate where swapping between metastable states becomes possible.

A necessary condition for the emergence of bistability[21] is that the free energy $G(r)$ is concave on some interval along r

$$\frac{\partial^2 G(r)}{\partial r^2} = K_m(r) + K < 0 \qquad (22)$$

where $K_m(r)$ is the second derivative of the molecular PMF $G_m(r)$. Therefore, given that $K_m(r) < 0$ in some region, if K_{min}

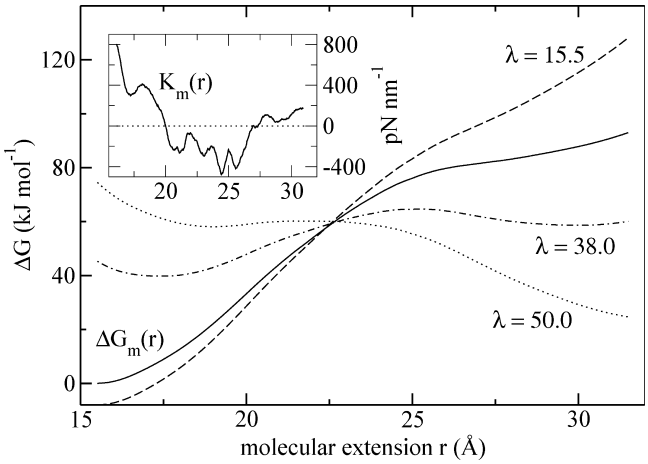

Figure 6. Free energy profile $G_m(r)$ of A_{10} in vacuo at $T = 300$ K is shown with a straight line, along with the potential of mean force $G_m(r) + V(r - \lambda)$ along r for different device positions. While for $\lambda = 15.5$ Å and $\lambda = 50.0$ Å the curves display a single minimum, corresponding respectively to the helical and extended state, for $\lambda = 38.0$ Å, the curve has a maximum that was not present in the original free energy $G_m(r)$. In the inset, the curvature $K_m(r)$ of $G_m(r)$ is shown.

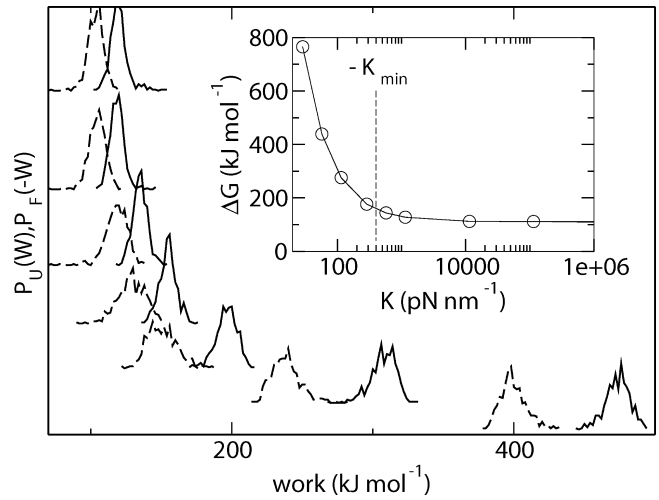

Figure 7. Unfolding and folding work distributions obtained for A_{10} in vacuo at $T = 300$ K at a constant pulling speed of 2.67 nm^{-1} ns^{-1} and at various device force constants K (56 000, 5600, 560, 280, 140, 56, 28 pN nm^{-1}, from top to bottom). In all experiments, the initial state and final states of the system are characterized by the end-to-end distances $r_F = 15.5$ and $r_U = 34.0$, respectively. In the inset, we report the free energy difference of the system plus device as a function of K.

denotes its minimum value in that region, the device force constant must satisfy the relation

$$K < -K_{min} \tag{23}$$

to induce bistability. The second derivative $K_m(r)$ of the PMF is shown in the inset of Figure 6, and the minimum of $K_m(r)$ is $K_{min} \sim -400$ pN nm^{-1}. Therefore, in the A_{10} case, for $K > 400$ pN nm^{-1}, there are no spurious metastable states along r for any λ value. When $K \gg -K_{min}$, at fixed values of λ, the equilibrium involves only the fast thermal modulation of the molecular degrees on a virtually fixed r coordinate. In these conditions, the reversibility/irreversibility of the experiments reflects the reversibility/irreversibility of the molecular system itself and the friction along the molecular extension coordinate due to the other degrees of freedom. The hysteresis in A_{10} in vacuo when driven by a stiff spring device is negligible already at $v = 1$ ns nm^{-1},[22] and the work distributions (see left panel in Figure 5) are sharply peaked near ΔG_m. Large hysteresis in force/extension cycles are systematically observed in the experimental practice.[3,7] The kinesin dimer, when pulled and compressed via AFM with force constant of the order of few pN nm^{-1}, exhibits a hysteresis (expressed as percentage of the forward work) of about 10%[7] at a speed as small as $v \simeq 5 \times 10^{-7}$ nm ns^{-1}. A single RNA hairpin with a loading rate of 7.5 pN s^{-1} using an optical trap returns a work that is 10% smaller in the refolding process with respect to the folding process.[3]

Experimentally observed force/extension cycles are strikingly similar to those obtained in the simulation of A_{10} in vacuo when $K \ll -K_{min}$ (see, e.g., Figure 4 right panel and Figure 1 of ref 3). In such conditions, the origin of the hysteresis in force/extension cycles is due not only to the presence of stiff barriers in $\Delta G_m(r)$, as suggested in ref 7, but also to the disparity between its second derivative $K_m(r)$ and the value of the device force constant. The dissipated work can hence depend strongly on the device stiffness. For example, as previously seen, at comparable pulling speed, the dissipation is a few kJ mol^{-1} when pulling with a stiff force constant while it is as large as 100 kJ mol^{-1} when pulling with a soft device (see Figures 4 and 5). This issue has been more thoroughly investigated by performing a series of simulations on A_{10} in vacuo using different values of the device force constant ($K = 560\,000$, 56 000, 5600, 560, 280, 140, 56, 28, and 14 pN nm^{-1}) at the fixed pulling speed of 2.67 nm ns^{-1}. For each value of the device force constant, we generated 512 trajectories in both directions. The starting folded (native) state, for all K, was sampled at regular time intervals of ~30 ps with control parameter set to $\lambda_F = 15.5$ Å corresponding to the mean value of the r coordinate in the unperturbed helical state. The final reference extended state was sampled at regular time intervals of ~30 ps using a K-dependent value of λ such that $r_U = 34.0$. The value of λ_U that forces the system to fluctuate around the selected reference extended state at $r_U = 34.0$ Å can be estimated from eq 17, obtaining $\lambda_U = 34.00$, 34.03, 34.31, 37.13, 40.26, 46.53, 65.32, 96.64, 159.28 Å for $K = 560\,000$, 56 000, 5600, 560, 280, 140, 56, 28, and 14 pN nm^{-1}, respectively.

The results of the nonequilibrium simulations on A_{10} in vacuo by varying the device force constant are conveyed in Figures 7 and 8. In Figure 7, the forward and reverse work distributions are shown for different K values. In the inset of Figure 7, we report the free energy difference ΔG between the final and initial state of the system calculated from the Bennett formula[23,24] as a function of K. When the bistability does not occur ($K > -K_{min}$), the system coordinate r always stays close to the device extension λ. In these conditions, the measured free energy difference does not depend on K and is practically coincident with the free energy difference of the pristine system even for K values close to the bistability limit. On the other hand, when $K < -K_{min}$, the measured free energy of the system plus device spring grows more than linearly with decreasing K in agreement with eq 16. Indeed, the solid line in the inset is given by eq 16 with $\Delta G_m = 111$ kJ mol^{-1} and $F_U = 176$ pN.

In the top panel of Figure 8, we report the mean work obtained in the unfolding−refolding cycle for various device force constant. As expected, the hysteresis is insignificant above the bistability threshold ($K > -K_{min}$) and grows as the device force constant decreases when $K > -K_{min}$. The hysteresis as a function of K obtained from the constant pulling speed bidirectional simulations is reported in the bottom panel of

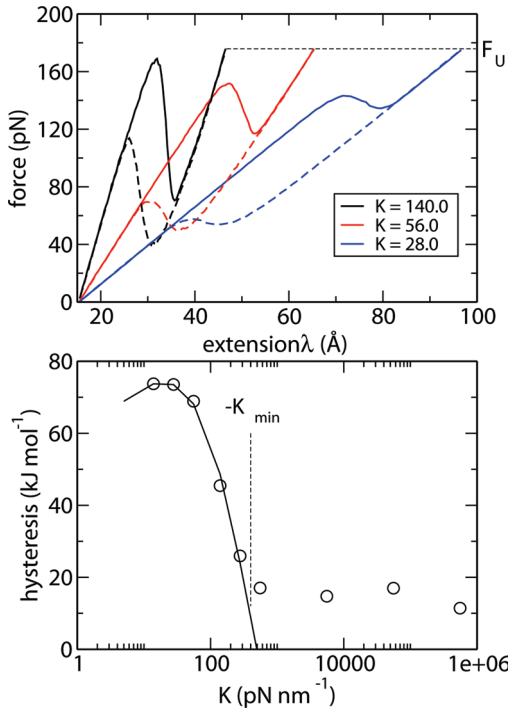

Figure 8. Results of a simulated force spectroscopy experiment on A_{10} at constant pulling speed of 2.67 nm^{-1} ns^{-1} and at various device force constants. Top panel: mean forward (solid line) and reverse (dashed line) force as a function of the device extension at $K = 28$, 56, and 140 pN nm^{-1}. Bottom panel: mean hysteresis in the force/extension cycles as a function of the device force constant.

Figure 8. The hysteresis is small and virtually constant for device force constant above the bistability threshold (even for values of K close to the threshold) and rapidly increases when passing from stiff to soft regime, due to the occurrence of the bistability along the end-to-end distance when $K < -K_{min}$. Equation 21 can be rewritten explicitly as a function of K as

$$h(K) = c + k_B T\left(\frac{r_{min} - r_F}{d}\right)\ln(K) + r_{min}^2\left(\frac{KK_m}{K + K_m}\right) \quad (24)$$

where following ref 2 we have assumed the force difference in eq 21 to depend logarithmically on the loading rate and therefore on the device stiffness K, and we have written K_{eff} explicitly. Since the second term on the right-hand side of eq 24 is a constant for $K_m \gg K$, the parameters c and d have been computed using the hysteresis values of the two simulations with the lower device stiffness, $K = 14$ and 28 pN nm^{-1}, obtaining $c = 57$ kJ mol^{-1} and $d = 0.36$ nm. The resulting curve is plotted in the bottom panel of Figure 8 and shows a good agreement with the simulated data (shown as circles) in the bistable ($K < 400$ pN nm^{-1}) regime.

We finally apply eq 7 to our force spectroscopy simulation data reported in Figure 4, which were obtained using the soft force constant $K = 56$ pN nm^{-1}. In order to recover ΔG_m, eq 7 corrects the free energy difference ΔG, directly measured from the work distributions via eq 3, with appropriate terms depending on the soft driving potential $V(r - \lambda)$ and the equilibrium probability density $P(r|\lambda)$. ΔG may be straightforwardly determined from the forward and reverse work probability reported in the left panel of Figure 4 by applying the Bennett acceptance ratio.[23,24] The accuracy of the Bennett formula depends on the

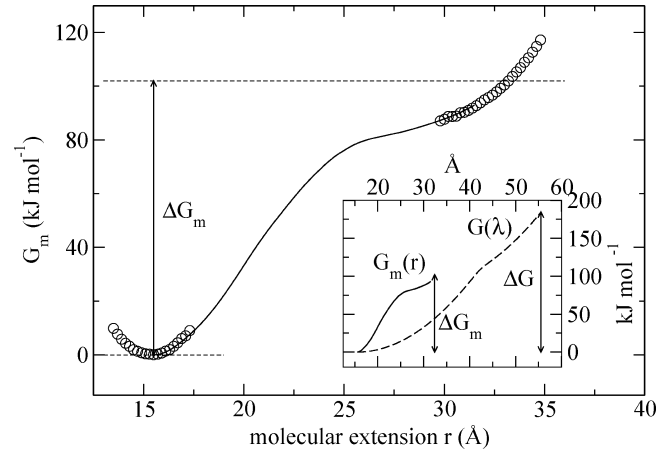

Figure 9. From the data reported in Figure 4, the free energy difference ΔG_m between the folded and extended states of A_{10} in vacuo at 300 K can be recovered from ΔG using eq 14. In the figure, the computed ΔG_m value is compared to the exact result obtained with thermodynamic integration. Moreover, the free energy profile $G_m(r)$ calculated near the maximum of the distributions $P(r|\lambda_F)$ and $P(r|\lambda_U)$ is shown with circles. In the inset, the free energy profile $G_m(r)$ is compared with reversible work $G(\lambda)$ to drive the device coupled to A_{10} along the coordinate λ.

pulling velocity (i.e., on the overlap of the forward and reverse work probability density) and on the number of forward and reverse nonequilibrium experiments. Clearly, as the statistics are unchanged in going from top to bottom in Figure 4, the best Bennett estimate for $\Delta G(\lambda)$ is obtained for the slowest pulling/pushing velocities. For $v = 0.33$ nm ns^{-1} ($\tau = 12$ ns), with $\lambda_F = 15.5$ and $\lambda_U = 55.5$, we obtain $\Delta G = 184$ kJ mol^{-1}. The average molecular extensions r_F and r_U at $\lambda_F = 15.5$ Å and $\lambda_U = 55.5$ Å are found to be 15.5 and 33.2 Å, respectively. $\Delta G_m = G_m(r_U) - G_m(r_F)$ is known exactly[11] for A_{10} in vacuo at $T = 300$ K and amounts to 102 kJ mol^{-1}. As already remarked by others,[14] we thus find that, in typical force spectroscopy experiments where $K_m \gg K$, ΔG may differ from ΔG_m by as much as 100%. The main contribution to the difference in eq 14, in the unfolding of a A_{10} molecule, comes from the term $\Delta V = V(r_U - \lambda_U) - V(r_F - \lambda_F) = 83.1$ kJ mol^{-1}, while the "entropic" correction is slightly negative, $k_B \ln P(r_U|\lambda_U) - k_B \ln P(r_F|\lambda_F) = -1$ kJ mol^{-1}. $G_m(r)$ can be recovered according to eq 7 for all r values for which the equilibrium probability densities $P(r|\lambda_F)$ and $P(r|\lambda_U)$ are appreciably nonzero. In Figure 9, we plot the reconstructed free energy $G_m(r)$ (circles) against the exact free energy of A_{10} in vacuo determined via thermodynamic integration (solid black line). The reconstruction of the full free energy profile $G_m(r)$ would require exponentially reweighing the configurations sampled at intermediate values of the position λ by the dissipated work and the application of the weighted histogram analysis method.[12,13] As we have shown, such an approach is unnecessary to recover the free energy difference ΔG_m between the native and unfolded states in bidirectional force spectroscopy experiments.

Conclusion

In this paper, we have done extensive nonequilibrium molecular dynamics simulation in a simple model system such as the alanine decapeptide in vacuo. By using a soft force constant of the order of few pN nm^{-1}, a typical value in AFM single-molecule experiments, we have been able to reproduce in a first series of bidirectional simulations the main features observed in real experiments. In particular, we have shown that

the coupling of a soft driving potential (a harmonic potential with force constant of the order of few pN nm^{-1}) with a typical PMF along the extension of a molecular system of interest leads to the large amount of hysteresis registered in the values of the irreversible work done to unfold and refold a macromolecule, during force spectroscopy experiments. Moreover, we have found that the free energy difference ΔG between the folded and unfolded states of the driven molecule, attainable via the application of the WFT to bidirectional works traces, can be as much as 100% larger than the original unfolding free energy ΔG_m of the free molecule, in agreement with recent experimental findings.[14] By performing a second series of simulation, this time at constant pulling speed and by varying the device force constant, we have shown that two regimes can be clearly identified: (i) in the "stiff" regime, that is, when the device force constant K is sufficiently large ($K > -K_{min}$), the free energy difference and the dissipated work are virtually independent of K; (ii) in the soft regime, that is, for K values such that $K < -K_{min}$, the apparent free energy grows with the inverse of K. We finally show how, for bidirectional unfolding/folding experiments done in the soft regime, the unfolding free energy of the free molecule can be recovered by using a simple and exact reweighting formula.

Acknowledgment. We gratefully acknowledge ENEA (Italian National Agency for New Technologies, Energy and Environment) for allowing access to the high-performance architectures of the CRESCO (Computational Research Center for Complex Systems) Project (http://www.cresco.enea.it). We wish to thank Samuele Pierattini of ENEA for his constant and competent technical support on the CRESCO facility.

References and Notes

(1) Marko, J. F.; Siggia, E. D. *Macromolecules* **1995**, *28*, 8759–8770.
(2) Izrailev, S.; Stepaniants, S.; Balsera, M.; Oono, Y.; Schulten, K. *Biophys. J.* **1997**, *72*, 1568–1581.
(3) Collin, D.; Ritort, F.; Jarzynski, C.; Smith, S. B.; Tinoco, I.; Bustamante, C. *Nature* **2005**, *437*, 231–234.
(4) Dudko, O. K.; Hummer, G.; Szabo, A. *Phys. Rev. Lett.* **2006**, *96*, 108101.
(5) Dudko, O. K.; Hummer, G.; Szabo, A. *Proc. Natl. Acad. Sci. U.S.A.* **2008**, *105*, 15755–15760.
(6) Greenleaf, W. J.; Woodside, M. T. *Annu. Rev. Biophys. Biomol.* **2007**, *36*, 171–190.
(7) Bornschloegl, T.; Woehlke, G.; Rief, M. *Proc. Natl. Acad. Sci. U.S.A.* **2008**, *106*, 6992–6997.
(8) Crooks, G. E. *J. Stat. Phys.* **1998**, *90*, 1481–1487.
(9) Crooks, G. E. *Phys. Rev. E* **2000**, *61*, 2361–2366.
(10) Park, S.; Schulten, K. *J. Chem. Phys.* **2004**, *120*, 5946–5961.
(11) Procacci, P.; Marsili, S.; Barducci, A.; Signorini, G. F.; Chelli, R. *J. Chem. Phys.* **2006**, *125*, 164101.
(12) Hummer, G. *J. Chem. Phys.* **2001**, *114*, 7330–7337.
(13) Minh, D. D. L.; McCammon, J. A. *J. Phys. Chem. B* **2008**, *112*, 5892–5897.
(14) Mossa, A.; de Lorenzo, S.; Huguet, J. M.; Ritort, F. *J. Chem. Phys.* **2009**, *130*, 234116.
(15) Kumar, S.; Bouzida, D.; Swendsen, R. H.; Kollman, P. A.; Rosenberg, J. M. *J. Comput. Chem.* **1992**, *13*, 1011–1021.
(16) Kosztin, I.; Barz, B.; Janosi, L. *J. Chem. Phys.* **2006**, *124*, 064106.
(17) Mackerell, A.; Bashford, D.; Bellot, M.; Dunbrack, R.; Evanseck, J.; Field, M.; Gao, J.; Guo, H.; Ha, S.; Joseph-Mcarthy, D.; Kuchnir, L.; Kuczera, K.; Lau, F.; Mattos, C.; Michnick, S.; Nog, T.; Nguyen, D.; Prodhom, B.; Reiher, W.; Roux, B.; Schlenkrich, M.; Smith, J.; Stote, R.; Straub, J.; Watanabe, M.; Wiorkiewicz-Kuczera, J.; Karplus, M. *J. Phys. Chem. B* **1998**, *102*, 3586–3616.
(18) Nose, S. *Mol. Phys.* **1984**, *52*, 255–268.
(19) Procacci, P.; Darden, T. A.; Paci, E.; Marchi, M. *J. Comput. Chem.* **1997**, *18*, 1848–1862.
(20) Marsili, S.; Signorini, G. F.; Chelli, R.; Marchi, M.; Procacci, P. *J. Comput. Chem.* In press.
(21) Franco, I.; Schatz, G. C.; Ratner, M. A. arXiv:0908.2208v1 [cond-mat.stat-mech], 2009.
(22) Marsili, S.; Procacci, P. arXiv:0904.3005 [cond-mat.stat-mech], 2009.
(23) Bennett, C. H. *J. Comput. Phys.* **1976**, *22*, 245.
(24) Shirts, M. R.; Bair, E.; Hooker, G.; Pande, V. S. *Phys. Rev. Lett.* **2003**, *91*, 140601.

JP908663Z